



HAL
open science

The role of small earthquakes in redistributing crustal elastic stress

David Marsan

► **To cite this version:**

David Marsan. The role of small earthquakes in redistributing crustal elastic stress. *Geophysical Journal International*, 2005, 163, pp.141-151. 10.1111/j.1365-246X.2005.02700.x . insu-00272288

HAL Id: insu-00272288

<https://insu.hal.science/insu-00272288>

Submitted on 19 Feb 2021

HAL is a multi-disciplinary open access archive for the deposit and dissemination of scientific research documents, whether they are published or not. The documents may come from teaching and research institutions in France or abroad, or from public or private research centers.

L'archive ouverte pluridisciplinaire **HAL**, est destinée au dépôt et à la diffusion de documents scientifiques de niveau recherche, publiés ou non, émanant des établissements d'enseignement et de recherche français ou étrangers, des laboratoires publics ou privés.

The role of small earthquakes in redistributing crustal elastic stress

D. Marsan

Laboratoire de Géophysique Interne et Tectonophysique, Université de Savoie, Le Bourget du Lac, France. E-mail: David.Marsan@univ-savoie.fr

Accepted 2005 April 27. Received 2005 March 15; in original form 2003 July 25

SUMMARY

Small-magnitude earthquakes have been shown to be negligible when estimating regional seismic moment release or seismic slip along major faults. However, they have a strong control on the redistribution of elastic stresses, and, according to statistical models of earthquake occurrences, on the triggering of subsequent earthquakes. This point is generally overlooked in stress-triggering model that only consider a limited set of earthquakes as stress sources. Elaborating on previous analyses, we here develop a probabilistic approach for estimating, at the hypocentre of an earthquake, the total stress caused by a large set of previous earthquakes, as a function of the magnitude range covered by these stress-generating earthquakes. A generic model that mimics the main features of earthquakes populations (most particularly: the Gutenberg–Richter relation and a fractal distribution of hypocentres with fractal dimension D) is constructed. The cumulative stresses generated in this model by sets of earthquakes are shown to follow a Lévy-stable law with stability index $D/3$. Similar conclusions are obtained when analysing the $M3+$ seismicity that occurred in southern California between 1981 and 2000. We show that the contribution to the cumulative static stress, caused by the occurrence of small earthquakes, at the site of pending earthquakes is at least as important as the contribution from the largest earthquakes. This is a direct consequence of the fractal clustering properties of earthquake hypocentre distributions. Including the stress redistribution due to small-scale seismicity should, therefore, significantly improve mechanical models of earthquake triggering.

Key words: aftershocks, earthquake triggering, Lévy laws, static stress.

1 INTRODUCTION

The role of small earthquakes in releasing the tectonic forces in the crust, is alternatively viewed as being either negligible or important.

Small earthquakes are negligible for slip/moment release:

The small magnitudes are found to contribute little to the overall seismic moment release and cumulative slip (Brune 1968; Scholz 1972, 1990; Scholz & Cowie 1990) and their contribution to the post-seismic relaxation can even be several orders of magnitude smaller than the one accommodated by afterslip (Shen *et al.* 1994). To summarize a simple argument, given the $M \sim 10^{1.5m}$ scaling of the seismic moment M with the magnitude m (Kanamori 1977; Hanks & Kanamori 1979), and the typical $N \sim 10^{-m}$ decay of the number N of earthquakes with m , one obtains that the total seismic moment released in the $[m_0 - \Delta m, m_0]$ magnitude band (m_0 being the largest magnitude characteristic of the fault zone) is $M_{[m_0 - \Delta m, m_0]} \sim \int_{m_0 - \Delta m}^{m_0} dm 10^{0.5m} \sim 1 - 10^{-0.5\Delta m}$. For $\Delta m = 2$, 90 per cent of the total moment is already accommodated, while this becomes 99 per cent for $\Delta m = 4$. There is, therefore, little need to consider earthquakes that are much smaller than the largest events when estimating the rate of moment release or of slip.

Possibly as a consequence of this (e.g. Parsons *et al.* 2000), along with the difficulty of incorporating more and more small earthquakes

in which source characteristics are not always well resolved, it has become customary in stress-modelling studies of earthquake occurrence to only consider a very limited set of earthquakes as controlling the stress redistribution responsible for the aftershocks (see Harris 1998; Stein 1999; King & Cocco 2001, for reviews). Such sets often consist of only one event, the main shock. A few studies (e.g. Harris *et al.* 1995; Jaumé & Sykes 1996; Deng & Sykes 1997; Nalbant *et al.* 1998; Ziv & Rubin 2000; King *et al.* 2001; Aoyama *et al.* 2002) have examined the stress changes caused by extended sets of earthquakes, but imposed generally high-magnitude cut-offs, sometimes for catalogue-completeness purposes. In most analyses, significant agreement between the modelled stress field and the distribution of subsequent earthquakes is observed. No analysis has been conducted as to what minimum size the magnitude interval for the sources should be, in order to make sure that most of the transferred stress is correctly modelled. An equivalent and still unresolved issue is whether one should consider earthquakes that occurred long before the start of an aftershock sequence as stress sources (see e.g. King *et al.* 2001, and how the aftershock sequence of the 1999 Izmit earthquake may have been conditioned by the 1963, M_s 6.4 Yalova earthquake).

Small earthquakes are important for stress release: It would, however, be erroneous to assume that elastic stress transfer is only

dominated by the largest events. Hanks (1992) showed that small ruptures can be expected to accommodate as much stress release over a fault as big ruptures, their number compensating for their weakness. Coming back to the above argument, this is now equivalent to summing $N \times M/L$ over the $[m_0 - \Delta m, m_0]$ interval (L being the characteristic length of the rupturing patch), where $M/L \sim 10^m$ possess the same scaling with m as the stress $\tau \sim u/L$ released by a magnitude m earthquake. This yields that $\Delta\sigma_{[m_0 - \Delta m, m_0]} \sim \Delta m$, that is, one cannot correctly estimate the total stress release by only considering the largest magnitudes. Felzer *et al.* (2002) and Helmstetter (2003) also noted that the clustering of earthquake hypocentres has to be accounted for when estimating the relative contribution versus size relation of stress interactions. Indeed, such a clustering implies that the stresses acting on a target, pending earthquake (hence, located on the cluster) or on a random target site (hence, not constrained to be on the cluster) should have very different distributions. A first proof of this result was given by Kagan (1994) who showed that the distribution of invariants of the stress increments caused by a fractal set of earthquakes with dimension D on subsequent earthquakes can be modelled by a Lévy-stable random variable (Feller 1971) with stability index $D/3$. For a site (earthquake) on the cluster, $D < 3$, while $D = 3$ for a random site. Such a change in the distribution is of crucial importance when summing up the influences of many earthquakes, since the rule for adding independent Lévy laws depends on the stability index.

The present paper aims at revising and interpreting the importance of earthquake clustering for elastic stress redistribution. We extend in Section 2 the analysis of Kagan (1994) to earthquake distributions with Gutenberg–Richter frequency–magnitude laws. The results are then compared in Section 3 to the distribution of stress changes for an extended set of earthquakes in southern California. Finally, we further discuss in Section 4 some of the assumptions made in this study, and interpret its meaning in relation to stress modelling of earthquake sequences.

2 THEORY

We estimate the probability distribution of σ , defined as the static shear stress generated by any given earthquake at the hypocentre or centroid of any future earthquake. The earthquakes are treated as double-couple point sources. The shear component of the stress along the rake direction of the future earthquake is analysed here, therefore, allowing to account for the geometries of both the causative and the target faults while bypassing the ambiguity on the nodal planes. Given the randomness in the relative geometries of the causative and the target faults, similar results hold with other scalar measures, as for example with stress invariants (see Section 3.3).

Knowing the distance r between the two hypocentres, the magnitude m of the first earthquake, and $\underline{\omega}$ a set of five angles specifying the geometry and the direction of the fault plane of the second earthquake relative to the position and geometry of the fault plane of the first earthquake (see Fig. 1), the far-field shear stress generated by the first earthquake at the hypocentre of the second is of the form

$$\sigma = CMr^{-3} \Phi(\underline{\omega}), \quad (1)$$

$$= C' u_m L_m^{-1} (r/L_m)^{-3} \Phi(\underline{\omega}), \quad (2)$$

where M is the seismic moment, u_m the mean displacement across the fault and L_m the typical size of a magnitude m earthquake, Φ a signed function $-1 \leq \Phi \leq 1$ corresponding to the modulation due to the radiation pattern and C and C' are two constants depending on

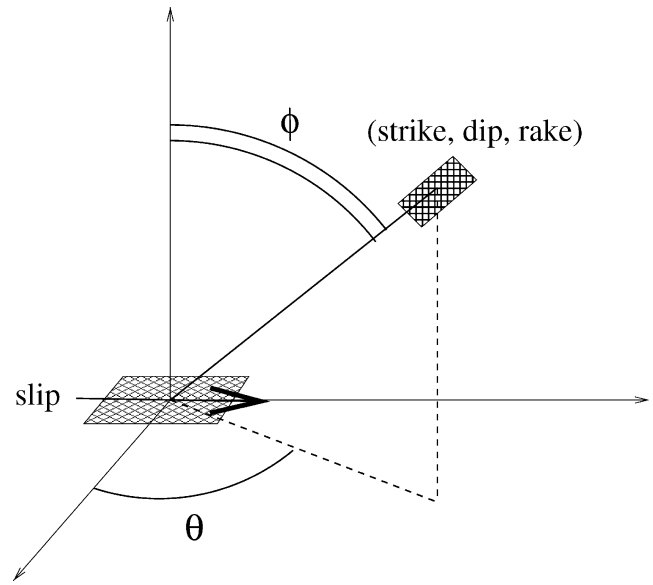


Figure 1. A set $\underline{\omega}$ of five angles: (θ, ϕ) , strike, dip and rake angles of the target fault, are needed to describe the direction and orientation of the target fault relative to the causative fault orientation (including direction of slip) and position.

material properties. In this section we set $C = C' = 1$, for simplicity. The moment scales as $M \sim 10^{1.5m} \sim \exp(\chi m)$ with $\chi = 1.5 \times \ln 10$ (Kanamori 1977; Hanks & Kanamori 1979).

We assume that the three variables r , m and $\underline{\omega}$ are random, following distributions (fractal, e.g. Kagan & Knopoff 1980; Robertson *et al.* 1995; exponential, i.e. Gutenberg–Richter, and uniform, respectively) that are typical of earthquake populations. While the geometries of the faults are certainly not random, we here consider that the orientation of the causative fault *as seen from the target fault* is random, hence a uniformly random $\underline{\omega}$ (cf. Fig. 1). This randomization is due to the random character of the relative position of the target fault versus the causative fault. Independence of these three random variables is also assumed. Based on these assumptions, we determine in Sections 2.1 and 2.2 the distributions of both:

- (1) $\sigma(m)$, the shear stress when the magnitude of the first earthquake is conditioned to be equal to m , while the distance r and the angles $\underline{\omega}$ are random (fractal and uniform, respectively); see Fig. 2(b);
- (2) σ , for r, m and $\underline{\omega}$ all random (fractal, exponential and uniform, respectively); see Fig. 2(c).

The total static shear stress originating from a large set of earthquakes is then calculated in Section 2.3, by summing $\sigma(m)$. Limits (i.e. for very large samples of earthquake populations) of sums of independent, identically distributed (iid) laws are more particularly examined in this latter section; such limits are largely insensitive to the details of the distributions given in Sections 2.1 and 2.2, and mostly depend on a few key parameters that statistically characterize the earthquake population (more particularly: fractal dimension and b -value). The contribution of the near-field stresses will be further discussed in Section 4.

2.1 Distribution of $\sigma(m)$, stress knowing m

We denote by $\sigma(m)$ the static shear stress individually caused by magnitude m earthquakes (see Fig. 2). This $\sigma(m)$ is random because

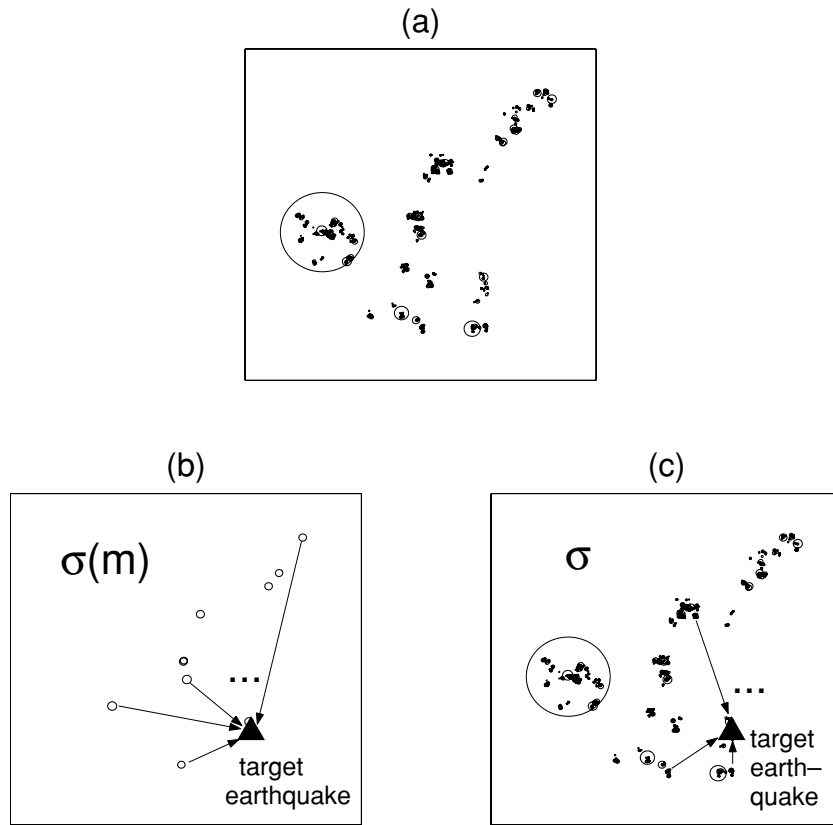


Figure 2. Schematic illustration of the two stress distributions $\sigma(m)$ and σ studied in Sections 2.1 and 2.2: (a) a realization of a model earthquake population, with magnitude following a Gutenberg–Richter distribution and epicentres clustered on a fractal set (with fractal dimension $D = 1$). The circles have radii exponentially increasing with the magnitude. (b) The stress $\sigma(m)$ is the random variable representing the stress generated by an earthquake of magnitude m at the site of a target earthquake. (c) The stress σ is the random variable representing the stress generated by an earthquake, with no constraint on its magnitude, at the site of a target earthquake.

both the distance r and the angles $\underline{\omega}$ are random. The distance r follows a fractal distribution, while $\underline{\omega}$ is uniformly distributed. The random variable $\Phi(\underline{\omega})$ can be shown to be well approximated by a Gaussian, for a uniform $\underline{\omega}$ random vector, in the point source approximation. While the departure from a Gaussian is strong as ones gets closer to the fault in the case of an extended source model, we only need to assume for the purpose of the present analysis that this distribution is symmetric; because it is defined over the interval $[-1, 1]$, it has a finite variance and zero mean, hence it is in the domain of attraction (for addition) of centred Gaussian laws.

The stress $\sigma(m, r) = \Phi(\underline{\omega}) \Sigma$ at fixed m and r is Gaussian, with standard deviation

$$\Sigma = u_m L_m^{-1} (r/L_m)^{-3} = M r^{-3}, \tag{3}$$

where $M = u_m L_m^2$ is the seismic moment. We now let r vary: the stress $\sigma(m)$ at a given (fixed) m is now a compound Gaussian random variable with random standard deviation $\Sigma = M s$ such that s is distributed according to r^{-3} , and M is a constant: $\sigma(m) = M s \Phi$. As stated earlier, we assume that the earthquake hypocentres are fractally distributed, with a fractal (correlation) dimension D . The probability density function (pdf) of the random variable r is, therefore, of the form $f_r(r) \sim r^{D-1}$, for r greater than a cut-off length. Given that $s \sim r^{-3}$, this yields that the pdf of s is $f_s(s) ds = f_r(r) dr$ hence $f_s(s) \sim s^{-1-D/3}$, that is, it follows a (skewed) Lévy-stable law with stability index $\alpha_1 = D/3$. The composition of such a law for the standard deviation $\Sigma = M s$ of $\sigma(m)$ and a zero-centred Gaussian law Φ implies that $\sigma(m)$ follows a symmetric Lévy-stable law

with $\alpha_1 = D/3$, at fixed m . We will denote this law as

$$\sigma(m) = \exp(\chi m) \mathcal{L}_{\alpha_1}, \tag{4}$$

with the seismic moment $M \sim \exp(\chi m)$ giving the dependence of $\sigma(m)$ on the magnitude, and \mathcal{L}_α denoting a unitary symmetric Lévy-stable law with stability index α (cf. Feller 1971). This result was first obtained by Kagan (1994), who calculated the distribution of the invariants of the stress tensor rather than the shear stress as is done here. As a short reminder, Lévy-stable laws are stable laws for the addition: the sum of independent Lévy-stable laws \mathcal{L}_α is itself a Lévy-stable law \mathcal{L}_α (up to a normalizing constant and recentering term). Given a_1, a_2, \dots, a_N a set of N real numbers, and X_1, X_2, \dots, X_N a set of N iid Lévy-stable laws \mathcal{L}_α , we have that:

$$a_1 X_1 + \dots + a_N X_N = (|a_1|^\alpha + \dots + |a_N|^\alpha)^{1/\alpha} \mathcal{L}_\alpha, \tag{5}$$

where the equality is in the distribution sense. The stability index α is such that $0 < \alpha \leq 2$. Index $\alpha = 2$ characterizing Gaussian laws, while $\alpha < 2$ corresponds to Lévy-stable laws with infinite variance. The mean also becomes infinite if $\alpha \leq 1$. For $\alpha < 2$, the stability index characterizing the tail of the pdf: if X is distributed according to \mathcal{L}_α , then its pdf is $f_X(x) \sim x^{-1-\alpha}$ at large x . The generalization of the central limit theorem to Lévy-stable laws states that the sum of N iid random variables X_1, \dots, X_N such that $f_X(x) \sim x^{-1-\alpha}$ at large x tends, in the limit of $N \rightarrow \infty$, to \mathcal{L}_α (still up to a normalizing constant). We refer the reader to Feller (1971) for a description of Lévy laws, their definitions and main properties. We abbreviate from now on ‘Lévy-stable’ to simply ‘Lévy’ laws.

2.2 Distribution of σ , for varying m , r and $\underline{\omega}$

We now relax the magnitude m , which is no longer constant but is now left to vary according to a Gutenberg–Richter law characterized by the b -value parameter. This is equivalent to saying that m is exponentially distributed, with a characteristic parameter $\beta = b/\ln 10$. Given our assumption of the independence of m and r , σ is the product of two independent random variables: the seismic moment $M \sim \exp(\chi m)$ and the Lévy law \mathcal{L}_{α_1} ; see eq. (4). The magnitude is distributed with a density $f_m(m) \sim \exp(-\beta m)$, yielding that the pdf of M is $f_M(M) \sim M^{-1-\beta/\chi}$, that is, the moment $M = \mathcal{L}_{\alpha_2}$ is a (skewed, positive) Lévy law with stability index $\alpha_2 = \beta/\chi$. While the product $\sigma = \mathcal{L}_{\alpha_1} \mathcal{L}_{\alpha_2}$ of two Lévy laws is not itself a Lévy law, it is however in the domain of attraction (for addition) of a Lévy law with index $\alpha = \min\{\alpha_1, \alpha_2\}$.

As the hypocentre of a pending earthquake undergoes the stresses generated by a great number of earlier earthquakes, and since each of those (shear) iid stresses is in the domain of attraction of a Lévy law with index $\alpha = \min\{\alpha_1, \alpha_2\}$, the cumulative stress at this site can be considered as being distributed according to such a Lévy law. Assuming a constant fractal dimension D , this stress will temporally evolve as $N^{1/\alpha}$, where N is the cumulative number of sources: the pdf of σ scales with N as $f_\sigma(\sigma) \sim N^{1/\alpha} L_\alpha$, with L_α the unitary, symmetric Lévy law of index α .

The value of α depends on the fractal dimension of the hypocentres D , the b value and the scaling law relating the seismic moment M to the magnitude m . Typical values of D (e.g. Goltz 1998) and b (e.g. Scholz 1990) are $D = 2$, $b = 1$, which, along with $\chi = 1.5 \ln 10$, yields $\alpha_1 = D/3 = 2/3$, $\alpha_2 = \beta/\chi = b/1.5 = 2/3$, hence $\alpha = \min\{\alpha_1, \alpha_2\} = 2/3$.

2.3 Summing the stress caused by a population of earthquakes

We now determine how the sum of all the stresses at a given location depends on the magnitude interval covered by the stress-generating earthquakes. We assume that only earthquakes with magnitude between magnitude $m_0 - \Delta m$ and a maximum magnitude m_0 can contribute to the total stress, denoted $\sigma[\Delta m]$. The goal is here to investigate whether increasing the magnitude interval Δm (by decreasing the cut-off $m_0 - \Delta m$) significantly change the total stress.

We assume that the earthquake population follows the Gutenberg–Richter relation, so that the earthquake density is $n(m) = N\beta \exp(-\beta m)$ where $\beta = b \ln 10$, N is the total number of earthquakes, and m is the magnitude above the magnitude of completeness. We denote by m_0 the magnitude of the biggest event; m_0 is a random variable, changing with every new earthquake population. It is known that the pdf of m_0 is $f_{m_0}(m_0) = N\beta(1 - e^{-\beta m_0})^{N-1} e^{-\beta m_0}$ (e.g. Feller 1971). One can then show that the mean of m_0 is well approximated, for sufficiently large N , by $E\{m_0\} = \frac{1}{\beta}(\ln N + \Gamma)$, where Γ is Euler's constant.

We first start by defining the total cumulative stress $\sigma[\Delta m|m_0]$ caused by all earthquakes with magnitude within Δm of the maximum magnitude m_0 , conditioned by the latter. This is equivalent to summing the stresses generated by these earthquakes at the target site, but only after selecting those earthquake populations that have the particular value m_0 as the magnitude of their biggest event.

Given that, for any individual earthquake of magnitude m , the generated stress is a Lévy random variable $\sigma(m) = \exp(\chi m) \mathcal{L}_{\alpha_1}$, where $\alpha_1 = D/3$ (cf. eq. 4), it comes that the sum of these stresses

is a stable integral (Samorodnitsky & Taquq 1994):

$$\sigma[\Delta m|m_0] = \left(\int_{m_0-\Delta m}^{m_0} dm n(m|m_0) e^{\alpha_1 \chi m} \right)^{1/\alpha_1} \mathcal{L}_{\alpha_1}, \quad (6)$$

where $n(m|m_0) = (N-1)\beta \frac{e^{-\beta m}}{1-e^{-\beta m_0}}$, for $0 \leq m \leq m_0$ (otherwise $n(m|m_0) = 0$) is the earthquake density conditioned by the maximum magnitude m_0 . Since $\sigma[\Delta m|m_0]$ is itself a Lévy law \mathcal{L}_{α_1} , it finally comes that

$$\sigma[\Delta m] = \left(\int_0^\infty dm_0 f_{m_0}(m_0) \sigma[\Delta m|m_0]^{\alpha_1} \right)^{1/\alpha_1} \mathcal{L}_{\alpha_1}, \quad (7)$$

where $f_{m_0}(m_0)$ is the pdf of m_0 already introduced above.

An important aspect in this development is that $\sigma[\Delta m]$ is defined as an ensemble average over an infinite number of earthquake populations. However, the situation is quite different when comparing these predictions to real data, as will be undertaken in Section 3: for a given case study, m_0 is set to a given value (the magnitude of the largest earthquake present in the data sets), which is generally higher than the unconditioned mean $E\{m_0\}$ as the seismicity sequences that include large and damaging earthquakes are more frequently studied than those with an average level of activity. This selection bias has for example been shown by Console *et al.* (2003) to be responsible for the large magnitude difference between the two largest earthquakes observed in typically selected seismicity catalogues/sequences. We, therefore, need to consider the conditioned $\sigma[\Delta m|m_0]$ of eq. (6) rather than $\sigma[\Delta m]$ of eq. (7). In order to estimate $\sigma[\Delta m]$ out of real data sets, one would need to consider seismicity distributions with no *a priori* selection bias.

We consider the stress $\sigma[\Delta m|m_0]$, for two cases of particular importance.

Case 1: A first case is considered, for which $D = 3$ hence $\alpha_1 = 1$. This corresponds to summing the stress at a uniformly random location (i.e. not necessarily at the hypocentre of an earthquake), or equivalently to summing the stress over a given crustal volume. Then eq. (6) becomes

$$\sigma[\Delta m|m_0] = \left(\int_{m_0-\Delta m}^{m_0} dm \frac{(N-1)\beta e^{-\beta m}}{1-e^{-\beta m_0}} e^{\chi m} \right) \mathcal{L}_1, \quad (8)$$

for $\Delta m < m_0$, and where \mathcal{L}_1 is the Cauchy law. This integral is equivalent to the sum of the seismic moments of all the earthquakes with magnitude in the interval $[m_0 - \Delta m, m_0]$, which is known to be dominated by large earthquakes/large faults (Brune 1968; Scholz & Cowie 1990). We get in this case that

$$\sigma[\Delta m|m_0] = (N-1) \frac{\beta}{\chi - \beta} \times \frac{e^{\chi m_0}}{e^{\beta m_0} - 1} [1 - e^{(\beta - \chi)\Delta m}] \mathcal{L}_1. \quad (9)$$

Since the stress only due to the largest earthquake (of magnitude m_0) is $\sigma^* = e^{\chi m_0} \mathcal{L}_1$, we see that the relative contribution (in terms of the scale factors multiplying the Cauchy law \mathcal{L}_1) of all the earthquakes in the interval $[m_0 - \Delta m, m_0]$, compared to the contribution of the largest earthquake with magnitude m_0 , is given by

$$\frac{\sigma[\Delta m|m_0]}{\sigma^*} = \frac{\beta}{\chi - \beta} \times \frac{N-1}{e^{\beta m_0} - 1} [1 - e^{(\beta - \chi)\Delta m}]. \quad (10)$$

For m_0 large enough compared to $\frac{1}{\chi - \beta}$, this ratio asymptotically increase from 0 to

$$\frac{\sigma_\infty}{\sigma^*} = \frac{\beta}{\chi - \beta} \times \frac{N-1}{e^{\beta m_0} - 1} \simeq \frac{\beta}{\chi - \beta} \times N e^{-\beta m_0}, \quad (11)$$

this asymptotic value being function of m_0 . As an illustration, Fig. 3 shows the ratio $\frac{\sigma_\infty}{\sigma^*}$ for southern California (1981–2000), as detailed

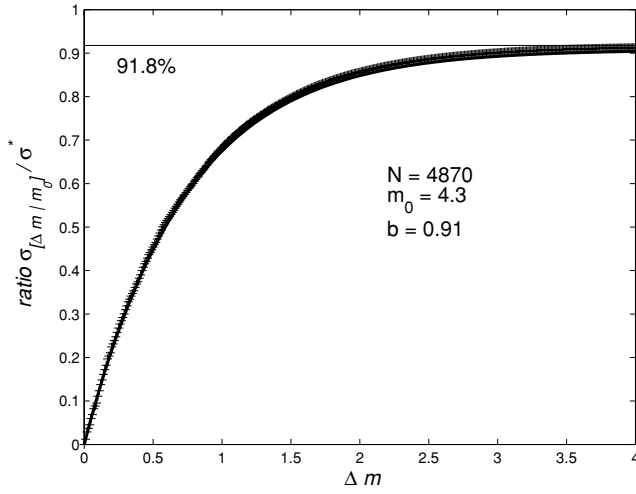


Figure 3. Ratio $\sigma[\Delta m|m_0]/\sigma^*$ function of Δm for $N = 4870$, $m_0 = 4.3$ and $b = 0.91$ as characterizing the seismicity data sets analysed in Section 3 (M3+ southern California earthquakes between 1981 and 2000). The crosses (+) show the mean of 1000 Monte Carlo simulations, and the continuous line is given by eq. (10). The ratio increases asymptotically to 0.918. For Δm greater than 2, at least 95 per cent of the total stress $\sigma[\Delta m|m_0]$ is correctly estimated.

in Section 3. Lowering the completeness magnitude by δm would correspond to (1) increasing the mean number of earthquakes by a factor $\exp(\beta\delta m)$, and (2) increasing m_0 to $m_0 + \delta m$ (since m_0 is defined as the maximum magnitude minus the completeness magnitude). The asymptotic value $\frac{\sigma_\infty}{\sigma^*}$ is therefore independent of the completeness magnitude, as long as N is large enough (i.e. permitting m_0 to be much larger than $\frac{1}{\chi - \beta}$).

The ratio $\frac{\sigma_\infty}{\sigma^*}$ is 2.105 for $b = 1$ and in the limit $N \rightarrow \infty$, when there is no constraint on m_0 , but can be much smaller if m_0 is constrained to large values. A strong correlation exists between m_0 and the difference h of magnitude between the two biggest earthquakes in the set. As shown by Console *et al.* (2003), if no constraint is put on m_0 , then h follows an exponential law with mean $E\{h\} = 1/\beta$ (Vere-Jones 1969), but this mean $E\{h\}$ increases if m_0 is constrained to be larger than a given threshold $m_0^* > 0$. The ratio $\frac{\sigma_\infty}{\sigma^*}$ can therefore be plotted versus $E\{h|m_0\}$; see Fig. 4 for an example with $N = 10^3$ and $b = 1$. Scholz (1972) mentions that 5 per cent of the seismic moment is typically released by the aftershocks. This value is however biased by the fact that typical case studies consider aftershock sequences following large main shocks, hence with an *a priori* constraint on h which becomes much larger than the unconstrained mean $E\{h\} \simeq 0.43$ (for $b = 1$). A similar claim is made by Shcherbakov & Turcotte (2004) for eight aftershock sequences in southern California, still with the same selection bias leading to a mean h of about 1.2. Fig. 4 shows that, for $b = 1$ and sets of $N = 10^3$ earthquakes, a value of $h = 1.2$ leads to $\frac{\sigma_\infty}{\sigma^*} \simeq 8.3$ per cent. This corresponds to choosing $m_0 \simeq 4.4$ on average, while the unconstrained mean of m_0 is 3.25 (still for $b = 1$ and $N = 10^3$).

We now show that the situation is very different when looking at the stress driving the seismicity, in particular the elastic stress resulting from earthquake interactions, as already pointed out by Hanks (1992).

Case 2: For a fractal dimension $D = 2$ and $b = 1$, we obtain that $\alpha_1\chi - \beta = 0$. These values for D and b are generally close to the values typically characterizing aftershock sequences. This

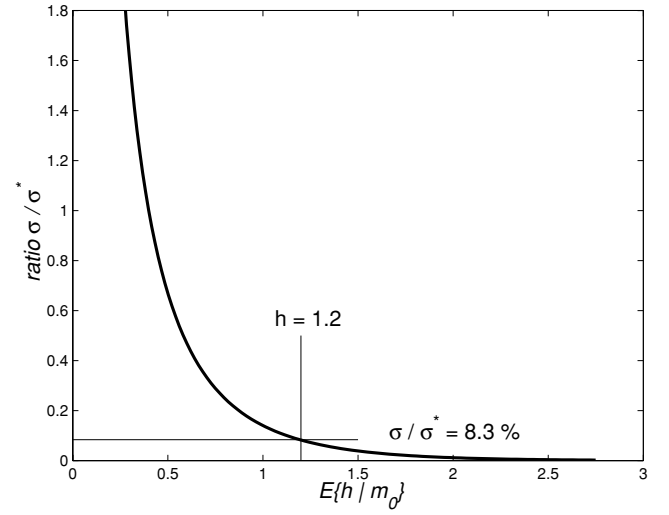


Figure 4. Ratio σ_∞/σ^* for $N = 10^3$ earthquakes and $b = 1$, function of the mean difference in magnitude $E\{h|m_0\}$ between the two largest earthquakes in the population. For $E\{h|m_0\} = 1.2$, as typically obtained for large historical sequences, the ratio is $\sigma_\infty/\sigma^* \simeq 0.083$. The unconstrained ratio, that is, for populations with no *a priori* on m_0 , is 2.105, for $b = 1$.

case of $\alpha_1\chi - \beta$ close to 0 is, therefore, often encountered when analysing earthquake populations. Unlike case 1, for which the stress $\sigma[\Delta m|m_0]$ was computed for a uniformly random site, this present case corresponds to examining the stress at the site of an impending earthquake. The distribution of $\sigma[\Delta m|m_0]$, therefore, characterizes the stress that drives the seismicity through elastic stress transfer following the occurrence of earthquakes. Eq. (6) now gives that

$$\sigma[\Delta m|m_0] = \left(\int_{m_0-\Delta m}^{m_0} dm \frac{(N-1)\beta}{1-e^{-\beta m}} \right)^{1/\alpha_1} \mathcal{L}_{\alpha_1}, \quad (12)$$

$$\Rightarrow \sigma[\Delta m|m_0] = \left[\frac{(N-1)\beta\Delta m}{1-e^{-\beta m_0}} \right]^{1/\alpha_1} \mathcal{L}_{\alpha_1}, \quad (13)$$

Hence, the ratio $\sigma[\Delta m|m_0]/\sigma^*$ is now

$$\frac{\sigma[\Delta m|m_0]}{\sigma^*} = \left[\frac{(N-1)\beta\Delta m}{e^{\alpha_1\chi m_0} - 1} \right]^{1/\alpha_1}. \quad (14)$$

This ratio grows as $\sim \Delta m^{1/\alpha_1}$ and is thus not bounded, see Fig. 5 for an example. The sign of $\alpha_1\chi - \beta$ is an important parameter in this analysis. This parameter gives the dependence of (number of earthquakes within a magnitude band around m) \times (the stress typically generated by an individual earthquake of magnitude m) with magnitude m . In case 1, $\alpha_1\chi - \beta > 0$ and the largest earthquakes are dominant. The small earthquakes then contribute little to $\sigma[\Delta m]$ and a cut-off magnitude can practically be defined to estimate this stress. On the contrary, for $\alpha_1\chi - \beta \leq 0$ (hence, including case 2), the small earthquakes contribute at least as much as the large ones, so that estimates of $\sigma[\Delta m]$ based on earthquake catalogues, for which there exists an observational magnitude cut-off, are not representative of the actual stress that drives the seismicity through stress transfer between earthquakes.

Case 2 is similar to the case considered by Hanks (1992), with $D = 2$ the (topological) dimension of a fault plane. Using $D = 2$, $\chi = 1.5 \times \ln 10$ and $b = 1$, he similarly obtained that all magnitude bands contributed equally in redistributing the forces over the fault surface. In the case of a rough fault surface $D > 2$, the same argument

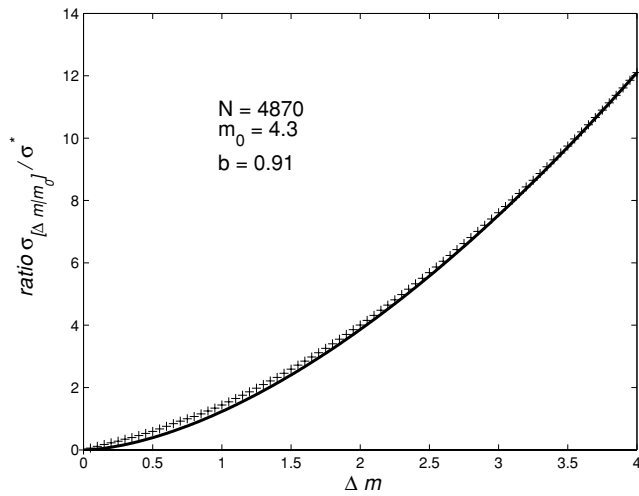


Figure 5. Same as Fig. 3, in the case $\alpha_1 \chi - \beta = 0 \Rightarrow \alpha_1 = 0.91/1.5 \simeq 0.61$. The continuous line is given by eq. (14).

as developed by Hanks (1992) leads to the prediction that the large events control the stress distribution. The typical case $D = 2.2$ (e.g. Schmittbuhl *et al.* 1995) gives that $\alpha_1 \chi - \beta = 0.23$.

The importance of the curvature of $\sigma[\Delta m]$ depends on the value of $\alpha_1 \chi - \beta$ compared to $1/\Delta m$. Dominance by the small or large magnitudes is therefore effective when $|\alpha_1 \chi - \beta| > \frac{1}{\Delta m} \Rightarrow |D/2 - b| > \frac{1}{\Delta m \ln 10}$. Taking $\frac{1}{\Delta m \ln 10} \simeq 0.1$ as a representative value of typical seismicity catalogues, this yields that all the magnitudes can be assumed to have an equal importance when $D = 2b \pm 0.2$. Such a condition is frequently verified, implying that seismicity catalogues are typically close to this critical case.

To summarize this section, we have shown that the stress caused by previous earthquakes is

(1) dominated by the largest earthquakes, if the target site is located at random in the upper crust or if the stress is averaged over a crustal volume. A good approximation of the total stress created at such a site is obtained by considering the largest earthquakes in a magnitude interval of about 2 (see Fig. 3) as sources. This total stress can however be substantially larger than the stress only caused by the largest earthquakes (see Fig. 4) so that a correct estimate of the stress effectively requires a sum over this magnitude interval, rather than only considering the largest earthquake as the only source that matters.

(2) not dominated by the largest earthquakes, if the target is the site of a future earthquake. This directly comes from the clustering of the earthquake hypocentres. It is found that small earthquakes are at least as important than large ones in creating stress on faults that will eventually rupture.

3 ANALYSES

3.1 Data

In this section we estimate the distributions of the stresses defined in Section 2, in the case of the seismicity that occurred in southern California between 1981 January 1 and 2000 December 31. The relocated data sets of Hauksson (2000) is analysed. The standard deviation of the location error for controlled sources (shots) is of the order of 0.4 km for horizontal coordinates and 1.4 km in depth (estimated from Fig. 9 of Hauksson 2000), along with a system-

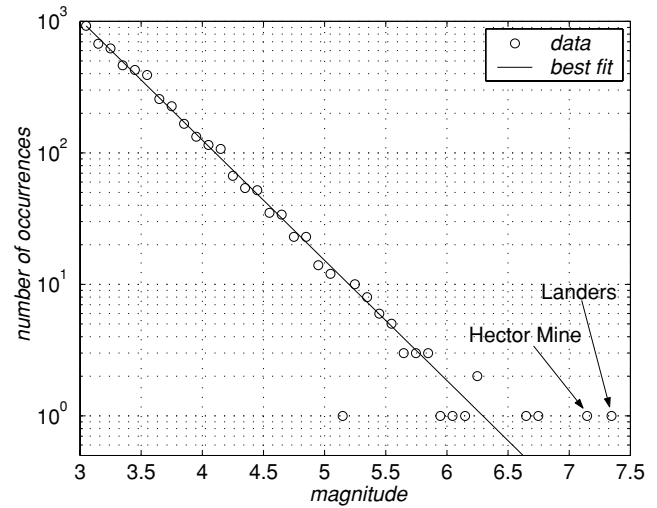


Figure 6. Number of occurrences versus magnitude for the selected sub-catalogue (20 yr of seismicity), along with the best Gutenberg–Richter law characterized by a b -value equal to 0.91 (method of Utsu 1966).

atic bias of about 1.2 km towards greater depths. As commented in Hauksson (2000), the typical mislocations for earthquakes are expected to be smaller than that for shots. However, the mean location errors, as listed in the data sets, are $\simeq 0.4$ km and $\simeq 4$ km for the horizontal and vertical coordinates, respectively. The mean depth is $\simeq 7.8$ km, with a standard deviation of about 4.4 km. Some events have badly constrained depths. A random depth following the depth distribution of the other earthquakes in the subset was drawn for those events. About 20 per cent of the earthquakes in the subset are given with more than one focal mechanism. A random selection was done to select only one solution for each of these events.

The magnitudes are mostly local or coda magnitudes except for the largest events for which a moment magnitude is estimated. Only earthquakes with magnitude greater or equal to 3 are analysed. Completeness of this subset is shown by the quality of the fit of the data with the Gutenberg–Richter law, with a b -value estimated to 0.91 (see Fig. 6). Out of 52 798 earthquakes originally listed in the catalogue, 4870 $M3+$ earthquakes are selected according to the aforementioned selection rules (i.e. magnitude above magnitude cut-off, and random selection of one focal mechanism when more than one is given).

The correlation integral (Grassberger & Procaccia 1983) is run on this set of earthquakes, *cf.* Fig. 7, in order to estimate the fractal dimension of the hypocentre set. It consists of counting the number $N(r)$ of pairs of earthquakes with hypocentral distance less than r . For a fractal set characterized by dimension D , $N(r)$ grows as r^D . Several breaks in the scaling are seen, which can be attributed to characteristic scales: at about 0.2 km (location error on latitude and longitude), at about 2 km (location error on depth), at about 10 km (thickness of the seismogenic zone) and at about 300 km (integral scale of the sample). Several scaling regimes are observed, in the scale intervals delimited by these characteristic scales: $D \simeq 2.2$ for $0.2 \text{ km} \leq r \leq 2 \text{ km}$, $D \simeq 1.7$ for $2 \text{ km} \leq r \leq 10 \text{ km}$, and $D \simeq 1.1$ for $10 \text{ km} \leq r \leq 300 \text{ km}$, where D is the fractal dimension. Those fractal dimensions are coherent with a 3-D self-similar distribution of hypocentres such that the probability distribution of X defined as the distance between any given pair of earthquakes projected along one coordinate axis scales as $f_X(x) \sim x^{-0.43}$. Such a scaling would yield $N(r) \sim r^{2.14}$, $\sim r^{1.7}$ and $\sim r^{1.14}$ in the 0.2–2 km, 2–10 km and 10–300 km intervals, respectively (see Appendix A). Among these

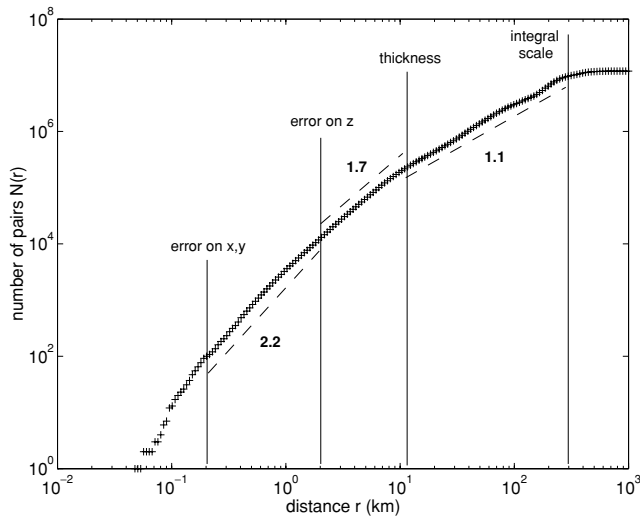


Figure 7. Number of pairs $N(r)$ of earthquakes separated by a distance less or equal to r . Four characteristic scales are observed, and the three scaling regimes identified are indicated along with an estimate of the corresponding fractal dimension.

four characteristic scales, only the 10 km scale related to the thickness of the schizosphere has a physical origin, while the others are artificial scales introduced by the location procedure and the size of the region under study. It can, therefore, be expected that the $N(r) \sim r^{1.7}$ regime actually extends to distances shorter than 0.2 km.

3.2 Distribution of $\sigma(m)$

The shear stress created by any earthquake i on any subsequent earthquake $j > i$ is computed, using the boundary element code of Gombert & Ellis (1994) that uses the dislocation solutions of Okada (1992) for the displacement and deformation. The true focal mechanisms as given in the data sets are used. The shear component of the stress is the one acting across the fault plane, in the slip (rake) direction of the target (subsequent) earthquake. The Poisson ratio is $\nu = 0.25$ and Young's modulus is $E = 70$ GPa. A constant stress drop is assumed for all the earthquakes. Denoting by u , L and W the mean slip, length and downdip width of the rupturing faults, we have that $u \sim L \sim W \sim 10^{0.5m}$ as long as W is less than 15 km. This transition occurs at $m \simeq 6.2$, after which $u \sim L \sim 10^{0.75m}$. The uniform slip u and the lengths L and W are further constrained by the mean slip $u \simeq 200$ cm and length $L \simeq 93$ km of the Landers earthquake. As an illustration, this choice of a scaling gives the values listed in Table 1 for several magnitudes.

Since the shear stress at $r = L$ is given by $\sigma_m(L) = C' \Phi u/L$, cf. eq. (2), and given that u and L are proportional to each other, this stress does not depend on m . The mean of $|\sigma_m(L)|$ over the set $\underline{\omega}$ of angles specifying the relative orientations of the two faults

Table 1. Average slip u , fault length L and width W function of magnitude m .

m	u (cm)	L (km)	W (km)
3	0.77	0.36	0.36
4	2.45	1.14	1.14
5	7.74	3.6	3.6
6	24.5	11.4	11.4
7	120	55.7	15

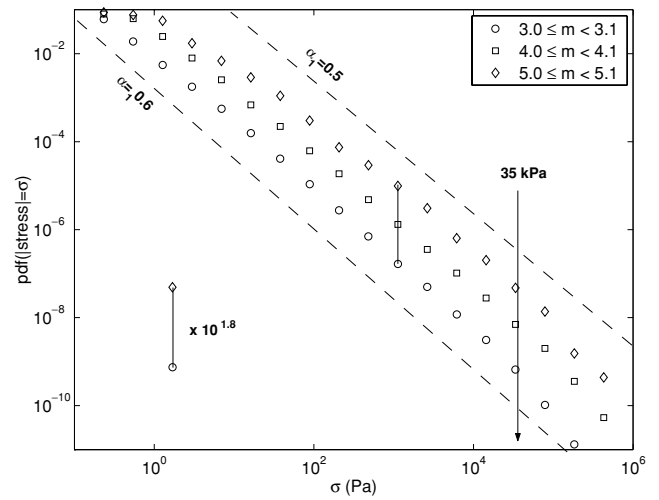


Figure 8. Probability density function of $|\sigma(m)|$, for three magnitude bands. The stress $\sigma(m)$ is due to all previous earthquakes of magnitude m , at the site of an earthquake. The pdf decays as $\sigma^{-1-\alpha_1}$ with α_1 estimated to 0.5–0.6 as shown by the dashed lines. In this scaling regime, a multiplication by $10^{1.8}$ is needed to obtain the pdf at $m + 2$ from the pdf at m (see text).

(cf. Fig. 1) is found to be $\simeq 35$ kPa for our choice of parameters. This 35 kPa stress value acts as an upper bound for the scaling regime characterizing the distributions of the stress. The exact value depends on our choice of elastic and material parameters, and is therefore only given here as a typical value rather than an absolute exact one. It marks the limit of validity of our point source model. We discuss in Section 4.2 the possibility that the $\sigma^{-1-\alpha_1}$ scaling regime of the stress pdfs actually extend to wider intervals, past the 35-kPa stress. Given the fact that the exact rupturing plane is not known, the extended source model used here only gives the correct order of magnitude of the imposed stress, as long as the hypocentral distances are larger than the causative fault length.

The distribution of $\sigma(m)$, the stress caused on an earthquake by all previous earthquakes of magnitude m , is shown in Fig. 8, for three magnitude bands [3.0, 3.1], [4.0, 4.1] and [5.0, 5.1]. The pdf is seen to decay following a $\sigma^{-1-\alpha_1}$ slope, with $\alpha_1 \simeq 0.5 - 0.6$ for all three magnitude bands. This value of $\alpha_1 = D/3$ is consistent with a fractal dimension $D = 1.7$ observed for the 2–10 km scale interval. This scaling regime of $N(r)$ extends over one decade in r , hence at least 3 decades in $\sigma(m)$ are expected to be characterized by this $\sigma^{-1-\alpha_1}$ decay. The calculated stresses are small compared to the ambient stress acting on tectonic faults, especially at depth where most of the seismicity occurs or nucleates. These relatively small fluctuations in stress caused by the occurrence of earthquakes are however expected to be effective in controlling the seismicity (e.g. King & Cocco 2001). An argument often proposed to explain this is that the crustal rocks in shear zones are stressed close to their critical state (Townend & Zoback 2000), so that small fluctuations can cascade into large instabilities (Bak & Tang 1989; Sornette & Sornette 1989; see also, among many others, Main 1996; Grasso & Sornette 1998). Also, these stresses distributed according to Fig. 8 are for individual sources. Summing over a large number of sources will strongly increase the stresses effectively caused by elastic stress transfer, especially since the role of small-magnitude events is of importance, as already discussed in Section 2.

The rupture length L plays here the role of yet another characteristic scale. It introduces a characteristic stress of about 35 kPa as mentioned above (for our choice of material and seismic source

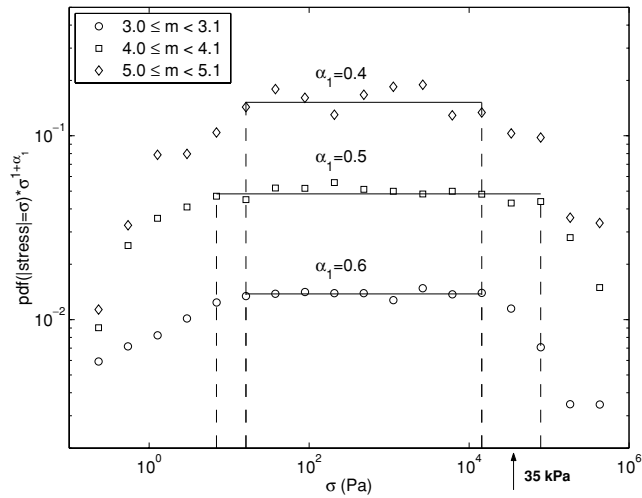


Figure 9. Same as Fig. 8, with the pdf of $|\sigma(m)|$ multiplied by $\sigma^{1+\alpha_1}$. The flat regimes (continuous lines) thus correspond to a pdf decaying as $\sigma^{-1-\alpha_1}$. The intervals to which this regime applies are delimited by the dashed lines. The exponent α_1 varies with the magnitude, as indicated on the graph.

parameters). The pdf of $|\sigma(m)|$ is clearly seen to experience a break of scaling at about this value, for the three magnitude bands. This break has a physical origin; for $r < L$, uniformity of the slip cannot be approximated any longer, and use of a generic slip distribution is needed; see Section 4.2 for further discussion on the near-field stress. This value of 35 kPa is less than 10^{-6} of the Young's modulus, and the plastic yield stress is, therefore, much larger than the interval characterized by this scaling regime.

The greater frequency of large $|\sigma(m)|$ at large m amounts to a simple multiplication of the pdf. Given the pdf f_1 of $|\sigma(m)|$ at m_1 , the pdf f_2 at $m_2 = m_1 + \delta m$ is obtained by $f_2(\sigma) = \lambda^{-1} f_1(\lambda^{-1} \sigma)$ with $\lambda = 10^{1.5\delta m}$. Since $f(\sigma) \sim \sigma^{-1-\alpha_1} \Rightarrow f_1(\sigma) = \lambda^{1+\alpha_1} f_1(\lambda^{-1} \sigma)$, we get that $f_2(\sigma) = 10^{1.5\alpha_1 \delta m} f_1(\sigma)$. For $\alpha_1 = 0.6$ and $\delta m = 2$ ($m_1 = 3, m_2 = 5$), this gives that $f_{m=5}(\sigma) = 10^{1.8} f_{m=3}(\sigma)$, in agreement with the observations, as shown by the vertical segment in Fig. 8.

A better picture of the scaling parameters and intervals associated with $\sigma(m)$ is given by Fig. 9, where the pdf are multiplied by $\sigma^{1+\alpha_1}$ with α_1 allowed to vary from one magnitude band to another. These variations of α_1 are significant, and can be attributed to the dependence of D on m (see Appendix B) which goes beyond our assumption that r and M are independent. The upper stress limit is clearly associated with the characteristic 35 kPa stress. Note that for $5 \leq m \leq 5.1$, the small number of sources causes some noisy fluctuations around the flat regime. For $m = 3$, the lower limit is due to the transition to the third scaling regime of the correlation integral (extending from the schizosphere thickness to the integral scale). A $\sigma^{-1.35}$ scaling regime for the pdf develops below this lower stress limit.

3.3 Distribution of σ

The distribution of σ , the shear stress created by any individual earthquake with no constraint on magnitude, at the site of subsequent earthquakes, is shown in Fig. 10. It is seen to follow a $\sigma^{-1.5}$ decay, indicative of a Lévy law with stability index $\alpha = 0.5$. This value is consistent with the prediction $\alpha = \min\{\alpha_1, \alpha_2\}$ of Section 2.2. In Section 3.2, α_1 was found to be in the range 0.5–0.6, and $\alpha_2 = \beta/\chi \simeq 0.61$. The pdf of σ is also plotted for the first stress invariant $\sigma_1 + \sigma_2 + \sigma_3$ rather than the shear stress, and for the shear stress after randomly reshuffling all the magnitudes. Both of these pdfs also

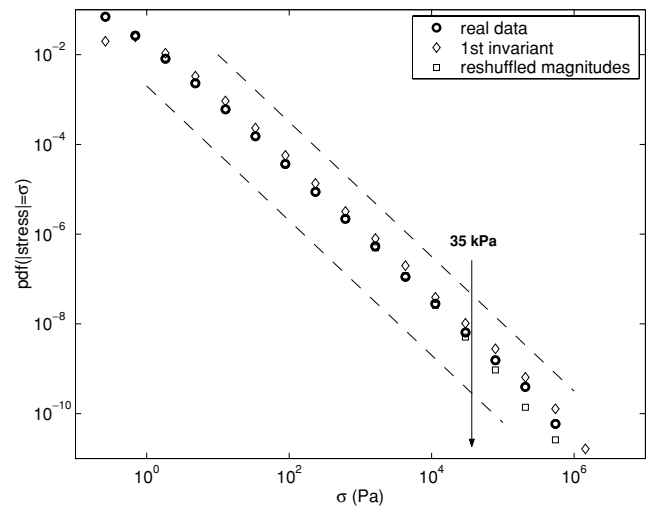


Figure 10. Probability density function of $|\sigma|$, the shear stress generated by one earthquake at the site of a future earthquake. The dashed lines correspond to $\sigma^{-1.5}$ power laws.

follow the $\sigma^{-1.5}$ scaling over the same stress interval, still bounded at about 35 kPa. By randomly reshuffling the magnitudes, we test how the hypothesis that r and M are independent affect the distribution of σ . In this test, the correlation integral $N(r)$ is by construction independent of m (apart from a multiplying factor), so that the power-law decay of the pdf of $|\sigma(m)|$ is the same at all m . The fact that the two pdfs (real data and reshuffled magnitudes) are nearly identical shows that the variations of α_1 with m have little influence on the scaling regime of σ . This comes from the greater number of small-magnitude events, the distribution of σ being strongly constrained by that of $\sigma(m)$ at low m .

3.4 Distribution of $\sigma_{[m_1, m_2]}$

In order to estimate the total stress exerted by all previous earthquakes with magnitudes $m_1 \leq m \leq m_2$ on subsequent earthquakes, denoted as $\sigma_{[m_1, m_2]}$, we divide the data sets in two parts. We keep the first 4670 earthquakes (out of a total of 4870, see Section 3.1) as stress sources, and use the last 200 earthquakes (nearly covering the whole of year 2000) as target sites. The latter are not considered as stress sources, so that all the target earthquakes receive stresses from the same set of earthquakes. We then compute, for each of those 200 faults, the total stress $\sigma_{[m_1, m_2]}$ by summing the stresses generated by all the stress sources with magnitude in four $[m_1, m_2]$ bands: [3.0, 4.0], [4.0, 5.0], [5.0, 6.0] and [6.0, 7.0].

Fig. 11 shows the four pdf. As described in Section 2.3, all magnitude bands have similar distributions, with the exception of $6 \leq m < 7$. We have $|D/2 - b| \simeq 0.06$ which is effectively smaller than 0.1 (*cf.* case 2 of Section 2.3). This result amounts to saying that the total contribution of all the earthquakes in a given magnitude band does not depend on the magnitude, but only on the size of the band. This situation was documented in case 2 of Section 2.3 and is expected to be commonly relevant to earthquake populations. This is a strong result, as it shows that one cannot *a priori* model the occurrence of earthquakes by only calculating the stress created by a few large earthquakes: the small-magnitude events are not negligible, their contribution in the total driving stress being comparable with the one of their largest counterparts. The consequences on stress interaction modelling are further discussed in Section 4.

A very different result is obtained when computing the total stress at random sites (latitude, longitude and depth were randomly drawn

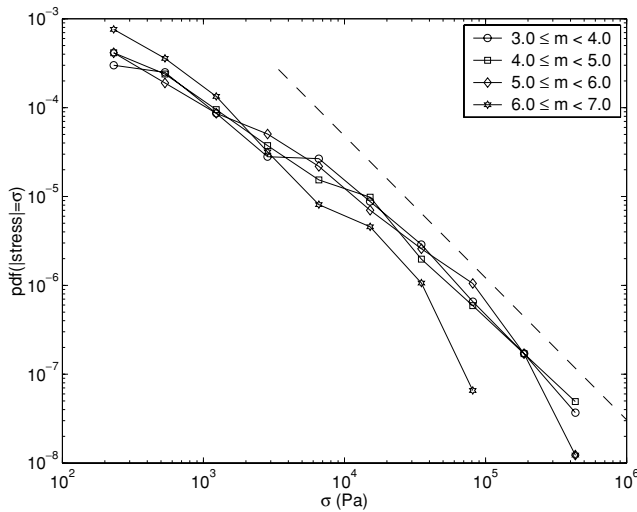


Figure 11. Probability density function of the stress $|\sigma_{[m_1, m_2]}|$ on an earthquake due to previous earthquakes with magnitude in the interval $[m_1, m_2]$, for four magnitude bands. The dashed line indicates a $\sigma^{-1.6}$ power law.

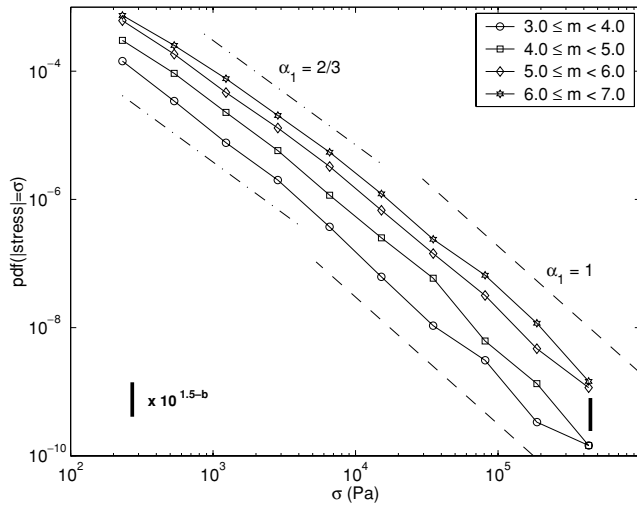


Figure 12. Probability density function of $|\sigma_{[m_1, m_2]}|$, the stress at random sites due to previous earthquakes with magnitude m in $[m_1, m_2]$, for four magnitude bands. The pdfs decay as σ^{-2} , hence $\alpha_1 = 1$, for large stress values (corresponding to an homogeneous 3-D distribution of nearby sources), while $\alpha_1 = 2/3$ for small stress (2-D distribution of remote, i.e. distances greater than the 15 km thickness of the schizosphere, sources). In theory one can go from the pdf at an interval $[m_1, m_2]$ to the pdf at another interval $[m_1 + 1, m_2 + 1]$ by multiplying it by $10^{1.5-b}$, as indicated by the thick bar.

as uniform laws, the first two in the $[31^\circ, 38^\circ]$, $[-121^\circ, -115^\circ]$ interval, depth in the 0–15 km interval), rather than at the site of future earthquakes. The same set of stress sources as above is kept. The corresponding pdfs of $\sigma_{[m_1, m_2]}$ are plotted in Fig. 12. As described in Section 2.3, case 1, the large magnitudes dominate this stress distribution. Eq. (8) gives that, for a constant magnitude bin width Δm , $\sigma_{[m, m+\Delta m]}$ should grow as $\exp[(\chi - \beta)m]$. This, along with a $f(|\sigma_{[m_1, m_2]}|) \sim \sigma^{-2}$ decay (as expected for $\alpha_1 = 1$) gives that this pdf at $m + 1$ can be deduced from the pdf at m by multiplying it by $\exp[(\chi - \beta)m] = 10^{1.5-b}$. This is in agreement with the pdfs shown in Fig. 12, with again the exception of the $6 \leq m < 7$ interval, in which only six events are counted.

4 DISCUSSION

4.1 Alteration of the stress field generated by a main shock and the modelling of aftershock triggering

As shown in Sections 2 and 3, the static stress caused by the main shock at sites of pending aftershocks undergoes significant alteration as the aftershock sequence develops. Most of the elastic stress transferred to faults that will eventually fail is due to small earthquakes, and is therefore difficult to model. To account for this transfer would imply the unrealistic task of modelling the stress redistribution following the occurrence of all the earthquakes in the sequence, down to very small magnitudes that are rarely or never detected by seismic networks (a cut-off magnitude lower than $m = -1$ being a possibility, see Abercrombie 1995). The relatively good agreement between stress maps calculated with just the main shock (or with a few large events) and off-fault seismicity distribution goes against this prediction. This agreement is often visual: mapping of the stress changes along with the seismicity typically shows a clear correlation between the two. The inclusion of smaller sources would not strongly alter the stress change map, as demonstrated by case 1 of Section 2.3 as it would correspond to volume averages of the stress. However, as is shown in Sections 2 and 3, earthquakes are observed to occur in clusters, so that, when estimating the elastic stress transferred from previous earthquakes to future earthquakes, the area of interest becomes much smaller than the total region shown on the map. The stresses caused by small shocks that look tiny and insignificant on the map, are of primary importance when studying elastic stress interactions.

A possible scenario that reconciliates both views can however be sketched. Early aftershock locations are constrained by the main shock stress redistribution. As more and more aftershocks occur in these early regions of stress increase, the stress in those regions undergo a strong alteration, while this alteration is weak in regions of early stress decrease. Aftershocks thus remain absent in regions where the main shock decreased the stress, while their repartition in regions where the main shock increased the stress is further conditioned by the aftershocks themselves. This can explain why large volumes of stress increase (caused by the main shock) are commonly observed to be devoid of seismicity. This type of fragmentation process is somewhat reminiscent of classical scale-invariant models (e.g. beta-model of Frisch *et al.* 1978) that lead to fractal clustering. Such a scenario implies that, since the distribution of aftershocks is constrained by the early stress decrease regions (caused by the main shock) and by the clustering of hypocentres in the regions of stress increase, the large-scale features of this distribution do not evolve much.

4.2 Near-field stress distribution

It was assumed in Sections 2 and 3 that the sources have uniform slip over the rupturing fault plane. This strongly limits the validity of the present analysis: along with the ambiguity on which of the two nodal planes is the causative one, it implies that the analysis is approximate and only gives the correct order of magnitude of the generated stresses. As a consequence, the distributions estimated in Section 3 possess a characteristic stress value of 35 kPa. More importantly, the predicted distributions are only valid in the far field, while numerous pairs of earthquakes have hypocentral distances shorter than the fault length of the first earthquake that occurred in the pair. It could, therefore, be a possibility that accounting for the near-field stress could severely modify the conclusions reached

here on the importance of small-size earthquakes in elastic stress interactions. We here give a tentative analysis of the near-field part of the stress distribution studied in this paper.

The $N(r) \sim r^D$, with $D = 1.7$, scaling of the correlation integral (Fig. 7) along with $L \sim e^{\chi m/3}$, gives that the number of earthquakes in the near field of an earthquake of magnitude m scales as $e^{D\chi m/3}$, and the total number of such near-field earthquakes for all earthquakes of magnitude m scales as $e^{(D\chi/3-\beta)m}$. This number increases with m if $D\chi/3 > \beta \Rightarrow D/2 > b$, which is not verified by the case study of Section 3. Again (as in Section 2.3, case 2), the parameter $|D/2 - b|$ is of particular importance here. As already argued, $D/2 - b$ is commonly close to 0 for many seismicity catalogues. This suggests that the number of target earthquakes located in the near field of earthquakes of magnitude m does not significantly vary with m .

The stress distribution close to the fault depends on the slip distribution; classical models of the latter (Aki & Richards 1980) have Gaussian statistics, though this assumption has yet to be thoroughly checked. Indeed, Lavallée & Archuleta (2003) have argued for a Lévy-stable slip distribution to characterize the 1979 Imperial Valley, California earthquake, with a stability index close to 1. It is difficult to reliably estimate such an index, given the sparsity of samples used to constrain this distribution. It has however to be noted that, for a Cauchy distribution (index equal to 1, see Feller 1971) of the slip and stress drop, the various contributions to the total static stress at the site of a pending earthquake in the near field simply sum up, and an argument equivalent to the one developed in Section 2 would here give that $\sigma_{[m_1, m_2]}^{\text{nearfield}} = \int_{m_1}^{m_2} dx p(x)$ with the probability density $p(m) \sim e^{-(D\chi/3-\beta)m}$. It is, therefore, a possibility that the same conclusions reached for the far-field (i.e. that the small-magnitude earthquakes play at least as important a role in creating stress at the sites of subsequent events as the large magnitude earthquakes do) also apply to the case of the near-field component. The stress distributions are then expected to exhibit a $\sigma^{-1-\alpha_1}$ decay over a wide stress interval, in particular extending past the 35 kPa value.

5 CONCLUSIONS

We have shown in this paper that small earthquakes are at least as important as large ones for creating static stress at the sites of pending earthquakes, although they can be neglected when considering volume averages (e.g. total seismic moment release) of the elastic stress changes. This, along with the previous observations (Felzer *et al.* 2002; see also Helmstetter 2003 who uses a declustering method to estimate the relation between the number of triggered earthquakes versus the magnitude of the trigger) indicates that small-scale seismicity plays an important part in the dynamics of earthquake populations, mostly because of the clustering properties of earthquake foci. During aftershock sequences, the stress field undergoes a significant alteration with the occurrence of many small events. However, this process may keep memory of the initial conditioning of the aftershock distribution by the main shock.

ACKNOWLEDGMENTS

I would like to thank Daniel Lavallée, three anonymous referees and the editor for their constructive reviews that helped improving and clarifying this contribution. This work was supported by a grant from the European Commission (PRESAP) under Framework Program 5.

REFERENCES

- Abercrombie, R.E., 1995. Earthquake source scaling relationships from -1 to $5 M_L$ using seismograms recorded at 2.5-km depth, *J. geophys. Res.*, **100**, 24 015–24 036.
- Aki, K. & Richards, P., 1980. *Quantitative Seismology*, W. H. Freeman, San Francisco.
- Aoyama, H., Takeo, M. & Ide, S., 2002. Evolution mechanisms of an earthquake swarm under the Hida Mountains, central Japan in 1998, *J. geophys. Res.*, **107**, 21 74, doi:10.1029/2001JB000540.
- Bak, P. & Tang, C., 1989. Earthquakes as a self-organized critical phenomenon, *J. geophys. Res.*, **94**, 15 635–15 637.
- Brune, J.N., 1968. Seismic moment, seismicity, and rate of slip along major fault zones, *J. geophys. Res.*, **73**, 777–784.
- Console, R., Lombardi, A.M., Murru, M. & Rhoades, D., 2003. Báth law and the self-similarity of earthquakes, *J. geophys. Res.*, **108**, 2128.
- Deng, J. & Sykes, L.R., 1997. Evolution of the stress field in southern California and triggering of moderate-size earthquakes: A 200-yr perspective, *J. geophys. Res.*, **102**, 9859–9886.
- Feller, W., 1971. *An Introduction to Probability Theory and Its Applications*, John Wiley and Sons, New York.
- Felzer, K.R., Becker, T.W., Abercrombie, R.E., Ekström, G. & Rice, J.R., 2002. Triggering of the 1999 M_w 7.1 Hector Mine earthquake by aftershocks of the 1992 M_w 7.3 Landers earthquake, *J. geophys. Res.*, **107**, 2190, doi:10.1029/2001JB000911.
- Frisch, U., Sulem, P.L. & Nelkin, M., 1978. A simple dynamical model of intermittent fully developed turbulence, *J. Fluid Mech.*, **87**, 719–736.
- Goltz, C., 1998. *Fractal and Chaotic Properties of Earthquakes*, Lecture notes in earth sciences, Springer, New York.
- Gomber, J. & Ellis, M., 1994. Topography and tectonics of the central New Madrid seismic zone: results of numerical experiments using a three-dimensional boundary element program, *J. geophys. Res.*, **99**, 20 299–20 310.
- Grassberger, P. & Procaccia, I., 1983. Characterization of strange attractors, *Phys. Rev. Lett.*, **50**, 346–349.
- Grasso, J.R. & Sornette, D., 1998. Testing self-organized criticality by induced seismicity, *J. geophys. Res.*, **103**, 29 965–29 987.
- Hanks, T.C., 1992. Small earthquakes, tectonic forces, *Science*, **256**, 1430–1432.
- Hanks, T.C. & Kanamori, H., 1979. A moment-magnitude scale, *J. geophys. Res.*, **84**, 2348–2352.
- Harris, R.A., 1998. Stress triggers, stress shadows, and implications for seismic hazard, *J. geophys. Res.*, **103**, 24 347–24 358.
- Harris, R.A., Simpson, R.W. & Reasenber, P.A., 1995. Influence of static stress changes on earthquake locations in southern California, *Nature*, **375**, 221–224.
- Hauksson, E., 2000. Crustal structure and seismicity distribution adjacent to the Pacific and North America plate boundary in southern California, *J. geophys. Res.*, **105**, 13 875–13 903.
- Helmstetter, A., 2003. Is earthquake triggering driven by small earthquakes?, *Phys. Rev. Lett.*, **91**, 058501.
- Jaumé S.C. & Sykes, L.R., 1996. Evolution of moderate seismicity in the San Francisco Bay region, 1850 to 1993: seismicity changes related to the occurrence of large and great earthquakes, *J. geophys. Res.*, **101**, 765–789.
- Kagan, Y.Y., 1991. Fractal dimension of brittle fracture, *J. Nonl. Sci.*, **1**, 1–16.
- Kagan, Y.Y., 1994. Distribution of incremental static stress caused by earthquakes, *Nonl. Pr. Geophys.*, **1**, 172–181.
- Kagan, Y.Y. & Knopoff, L., 1980. Spatial distribution of earthquakes: the two-point correlation function, *Geophys. J. R. astr. Soc.*, **62**, 303–320.
- Kanamori, H., 1977. The energy release in great earthquakes, *J. geophys. Res.*, **82**, 2981–2987.
- King, G.C.P. & Cocco, M., 2001. Fault interaction by elastic stress changes: new clues from earthquake sequences, *Adv. Geophys.*, **44**, 1–38.
- King, G.C.P., Hubert-Ferrari, A., Nalbant, S.S., Meyer, B., Armijo, R. & Bowman, D., 2001. Coulomb interactions and the 17 August 1999 Izmit, Turkey earthquake, *C. R. Acad. Sci. Paris, Sér. 2*, **333**, 557–569.

Lavallée, D. & Archuleta, R.J., 2003. Stochastic modeling of slip spatial complexities for the 1979 Imperial Valley, California, earthquake, *Geophys. Res. Lett.*, **30**, 1245, doi:10.1029/2002GL015839.

Main, I., 1996. Statistical physics, seismogenesis, and seismic hazard, *Rev. of Geophys.*, **34**, 433–462.

Marsan, D., Bean, C.J., Steacy, S. & McCloskey, J., 2000. Observation of diffusion processes in earthquake populations and implications for the predictability of seismicity systems, *J. geophys. Res.*, **105**, 28 081–28 094.

Marsan, D. & Bean, C.J., 2003. Seismicity response to stress perturbations, analysed for a world-wide catalogue, *Geophys. J. Int.*, **154**, 179–195.

Nalbant, S.S., Hubert, A. & King, G.C.P., 1998. Stress coupling between earthquakes in northwest Turkey and the north Aegean Sea, *J. geophys. Res.*, **103**, 24 469–24 486.

Okada, Y., 1992. Internal deformation due to shear and tensile faults in a half-space, *Bull. seism. Soc. Am.*, **82** 1018–1040.

Parsons, T., Toda, S., Stein, R.S., Barka, A. & Dieterich, J.H., 2000. Heightened odds of large earthquakes near Istanbul: an interaction-based probability calculation, *Science*, **288**, 661–665.

Robertson, M.C., Sammis, C.G., Sahimi, M. & Martin, A.J., 1995. Fractal analysis of three-dimensional spatial distributions of earthquakes with a percolation interpretation, *J. geophys. Res.*, **100**, 609–620.

Samorodnitsky, G. & Taquq, M.S., 1994. *Stable non-Gaussian random processes*, Chapman & Hall, New York.

Schmittbuhl, J., Schmitt, F. & Scholz, C., 1995. Scaling invariance of crack surfaces, *J. geophys. Res.*, **100**, 5953–5973.

Scholz, C.H., 1972. Crustal movements in tectonic areas, *Tectonophysics*, **14**, 201–217.

Scholz, C.H., 1990. *The mechanics of earthquakes and faulting*, Cambridge Univ. Press, Cambridge.

Scholz, C.H. & Cowie, P.A., 1990. Determination of total strain from faulting using slip measurements, *Nature*, **346**, 837–839.

Shcherbakov, R. & Turcotte, D.L., 2004. A modified form of Bath's law, *Bull. seism. Soc. Am.*, **94**, 1968–1975.

Shen, Z.-K., Jackson, D.D., Feng, Y., Cline, M., Kim, M., Fang, P. & Bock, Y., 1994. Postseismic deformation following the Landers earthquake, California, 28 June 1992, *Bull. seism. Soc. Am.*, **84**, 780–791.

Sornette, D. & Sornette, A., 1989. Self-organized criticality and earthquakes, *Europhys. Lett.*, **9**, 197–202.

Stein, R.S., 1999. The role of stress transfer in earthquake occurrence, *Nature*, **402**, 605–609.

Townend, J. & Zoback, M.D., 2000. How faulting keeps the crust strong, *Geology*, **28**, 399–402.

Utsu, T., 1966. A statistical significance test of the difference in *b*-value between two earthquake groups, *J. Phys. Earth*, **14**, 37–40.

Vere-Jones, D., 1969. A note on the statistical interpretation of Bath's law, *Bull. seism. Soc. Am.*, **59**, 1535–1541.

Ziv, A. & Rubin, A.M., 2000. Static stress transfer and earthquake triggering : no lower threshold in sight?, *J. geophys. Res.*, **105**, 13 631–13 642.

APPENDIX A: SCALING REGIMES ASSOCIATED WITH A SELF-SIMILAR SET OF HYPOCENTRES

We consider a 3-D self-similar distribution of hypocentres, such that the probability density function (pdf) of the separation length

X between two hypocentres projected along any coordinate axis is $f_X(x) \sim x^{-a}$. Self-similarity implies scaling isotropy. The pdf $f_R(r)$ of the distance r is then scaling according to

$$f_R(r) = \int dx f_X(x) \int dy f_Y(y) \int dz f_Z(\sqrt{r^2 - x^2 - y^2}) \quad (A1)$$

hence $f_R(r) \sim r^{2-3a}$ as obtained following the change of coordinates $u = x/r, v = y/r$. This yields that the number of pairs $N(r)$ separated by a distance between 0 and r scales as

$$N(r) \sim \int_0^r ds f_R(s) \sim r^{3-3a}. \quad (A2)$$

This self-similarity is only valid in the 2–10 km interval, that is, above the error scale on depth and below the characteristic thickness of the schizosphere (cf. Fig. 7). We thus have $3 - 3a \simeq 1.7 \Rightarrow a \simeq 0.43$. For $0.2 \text{ km} \leq r \leq 2 \text{ km}$, the separation z in depth follows a uniform distribution, hence $f_Z(z) \sim z^0$ which leads to $N(r) \sim r^{3-2a}$, hence, a fractal dimension predicted to be equal to 2.14. Finally, the scaling in the 20–300 km interval is obtained by projecting the 3-D hypocentre set on the (x, y) plane, giving the epicentre distribution, hence

$$f_R(r) = \int dx f_X(x) \int dy f_Y(\sqrt{r^2 - x^2}) \sim r^{1-2a}. \quad (A3)$$

This gives that $N(r) \sim r^{2-2a}$, yielding $D = 1.14$ for $a = 0.43$.

APPENDIX B: DEPENDENCE OF THE FRACTAL DIMENSION D ON THE MAGNITUDE M AND THE TIME INTERVAL T

A constant fractal dimension D for the hypocentre distribution is assumed in Section 2. The analyses of Section 3 however show that D depends on the conditional magnitude of the first earthquake of the pair. Also, dependence of D on the duration T of the catalogue (Kagan & Knopoff 1980; Kagan 1991) or on the number of samples (see Robertson *et al.* 1995, for the capacity dimension) has been documented. Systematic changes of the spatial structure of temporally correlated earthquake distribution with timescale (Marsan *et al.* 2000; Marsan & Bean 2003) can explain these observations. As a consequence, the stability indices α_1 and α characteristic of the distributions of $\sigma(m)$ and σ should depend on both m and T . Since the summation of eq. (6) assumes a constant D with m , it can only serve as a first order approximation of the real distribution of the total stress $\sigma_{[m_1, m_2]}$. As the timescale T increases to very long (geological) scales, D hence also α_1 increase. However, the index α of σ , defined as $\alpha = \min\{\alpha_1, \alpha_2\}$ with $\alpha_2 = \beta/\chi = b/1.5$ (see Section 2.2) stays constant if one assumes a relatively constant b -value.